Thermal properties of borate crystals for high power optical parametric chirped-pulse amplification

R. Riedel,[1,*] J. Rothhardt,[1,2] K. Beil,[3,4] B. Gronloh,[5] A. Klenke,[1,2]
H. Höppner,[6] M. Schulz,[6] U. Teubner,[7,8] C. Kränkel,[3,4] J. Limpert,[1,2]
A. Tünnermann,[1,2] M.J. Prandolini,[1] and F. Tavella[1]

[1] *Helmholtz-Institut Jena, Fröbelstieg 3, D-07743 Jena, Germany*
[2] *Institute of Applied Physics, Abbe Center of Photonics, Friedrich-Schiller-University Jena, Albert-Einstein-Straße 15, D-07745 Jena, Germany*
[3] *Institut für Laserphysik, Universität Hamburg, Luruper Chaussee 149, D-22761 Hamburg, Germany*
[4] *The Hamburg Centre for Ultrafast Imaging, Luruper Chaussee 149, D-22761 Hamburg, Germany*
[5] *Fraunhofer Institute for Laser Technology, Steinbachstraße 15, D-52074 Aachen, Germany*
[6] *Deutsches Elektronensynchrotron DESY, Notkestraße 85, D-22607 Hamburg, Germany*
[7] *Institut für Lasertechnik Ostfriesland, Hochschule Emden, Constantiaplatz 4, D-26723 Emden, Germany*
[8] *Institut für Physik, Carl von Ossietzky Universität Oldenburg, Ammerländer Heerstraße 114–118, D-26129 Oldenburg*

[*] *robert.riedel@desy.de*

Abstract: The potential of borate crystals, BBO, LBO and BiBO, for high average power scaling of optical parametric chirped-pulse amplifiers is investigated. Up-to-date measurements of the absorption coefficients at 515 nm and the thermal conductivities are presented. The measured absorption coefficients are a factor of 10–100 lower than reported by the literature for BBO and LBO. For BBO, a large variation of the absorption coefficients was found between crystals from different manufacturers. The linear and nonlinear absorption coefficients at 515 nm as well as thermal conductivities were determined for the first time for BiBO. Further, different crystal cooling methods are presented. In addition, the limits to power scaling of OPCPAs are discussed.

OCIS codes: (190.4400) Nonlinear optics, materials; (190.4410) Nonlinear optics, parametric processes; (140.3280) Laser amplifiers.

References and links

1. A. Dubietis, G. Jonušauskas, and A. Piskarskas, "Powerful femtosecond pulse generation by chirped and stretched pulse parametric amplification in BBO crystal," Opt. Commun. **88**, 437–440 (1992).
2. I. N. Ross, P. Matousek, M. Towrie, A. J. Langley, and J. L. Collier, "The prospects for ultrashort pulse duration and ultrahigh intensity using optical parametric chirped pulse amplifiers," Opt. Commun. **144**, 125–133 (1997).
3. R. Butkus, R. Danielius, A. Dubietis, A. Piskarskas, and A. Stabinis, "Progress in chirped pulse optical parametric amplifiers," Appl. Phys. B **79,** 693–700 (2004).
4. R. Riedel, A. Stephanides, M. J. Prandolini, B. Gronloh, B. Jungbluth, T. Mans, and F. Tavella, "Power scaling of supercontinuum seeded megahertz-repetition rate optical parametric chirped pulse amplifiers," Opt. Lett. **39,** 1422–1424 (2014).

#206255 - $15.00 USD Received 18 Feb 2014; revised 8 May 2014; accepted 8 May 2014; published 14 Jul 2014

5. J. Rothhardt, S. Demmler, S. Hädrich, J. Limpert, and A. Tünnermann, “Octave-spanning OPCPA system delivering CEP-stable few-cycle pulses and 22 W of average power at 1 MHz repetition rate,” Opt. Express **20**, 10870–10878 (2012).
6. R. Riedel, M. Schulz, M.J. Prandolini, A. Hage, H. Höppner, T. Gottschall, J. Limpert, M. Drescher, and F. Tavella, “Long-term stabilization of high power optical parametric chirped-pulse amplifiers,” Opt. Express **21**, 28987–28999 (2013).
7. T. Eidam, S. Hanf, E. Seise, T. V. Andersen, T. Gabler, C. Wirth, T. Schreiber, J. Limpert, and A. Tünnermann, “Femtosecond fiber CPA system emitting 830 W average output power,” Opt. Lett. **35,** 94–96 (2010).
8. P. Russbueldt, T. Mans, J. Weitenberg, H. D. Hoffmann, and R. Poprawe, “Compact diode-pumped 1.1 kW Yb:YAG Innoslab femtosecond amplifier,” Opt. Lett. **35,** 4169–4171 (2010).
9. A. Giesen and J. Speiser, “Fifteen Years of Work on Thin-Disk Lasers: Results and Scaling Laws,” IEEE Sel. Top. in Quantum Elec. **13,** 598–609 (2007).
10. T. Metzger, A. Schwarz, C.Y. Teisset, D. Sutter, A. Killi, R. Kienberger, and F. Krausz, “High-repetition-rate picosecond pump laser based on a Yb:YAG disk amplifier for optical parametric amplification,” Opt. Lett. **34,** 2123–2125 (2009).
11. G. Sansone, F. Calegari, and M. Nisoli, “Attosecond Technology and Science,” IEEE J. Sel. Top. in Quantum Elec. **18**, 507–519 (2012).
12. S. Banerjee, M. Baudisch, J. Biegert, A. Borot, A. Borzsonyi, D. Charalambidis, T. Ditmire, Zs. Diveki, P. Dombi, K. Ertel, M. Galimberti, J. A. Fülöp, E. Gaul, C. Haeffner, M. Hemmer, C. Hernandez-Gomez, M. Kalashnikov, D. Kandula, A. P. Kovacs, R. Lopez-Martens, P. Mason, I. Márton, I. Musgrave, K. Osvay, M. Prandolini, E. Racz, P. Racz, R. Riedel, I. N. Ross, J.-P. Rosseau, M. Schulz, F. Tavella, A. Thai, I. Will, “Conceptual design of the laser system for the attosecond light pulse source,” in CLEO:2013 Technical Digest © OSA, (2013).
13. M. J. Prandolini, R. Riedel, M. Schulz, A. Hage, H. Höppner, and F. Tavella, “Design considerations for a high average power, ultrabroadband, optical parametric chirped-pulse amplifier,” Opt. Express **22,** 1594–1607 (2014).
14. J. Rothhardt, S. Demmler, S. Hädrich, T. Peschel, J. Limpert, and A. Tünnermann, “Thermal effects in high average power optical parametric amplifiers,” Opt. Lett. **38,** 763–765 (2013).
15. V. Petrov, M. Ghotbi, O. Kokabee, A. Esteban-Martin, F. Noack, A. Gaydardzhiev, I. Nikolov, P. Tzankov, I. Buchvarov, K. Miyata, A. Majchrowski, I.V. Kityk, F. Rotermund, E. Michalski, and M. Ebrahim-Zadeh, “Femtosecond nonlinear frequency conversion based on BiB_3O_6,” Laser & Photon. Rev. **4,** 53–98 (2010).
16. R. Akbari and A. Major, “Optical, spectral and phase-matching properties of BIBO, BBO and LBO crystals for optical parametric oscillation in the visible and near-infrared wavelength ranges,” Laser Phys. **23**, 035401 (2013).
17. Z.M. Liao, I. Jovanovic, C.A. Ebbers, Y. Fei, and B. Chai, “Energy and average power scalable optical parametric chirped-pulse amplification in yttrium calcium oxyborate,” Opt. Lett. **31,** 1277–1279 (2006).
18. A. V. Smith, *SNLO nonlinear optics code (Ver. 60)*, AS-Photonics, Albuquerque, USA (2013).
19. R. H. French, J. W. Ling, F. S. Ohuchi, and C. T. Chen, “Electronic structure of β-BaB_2O_4 and LiB_3O_5 nonlinear optical crystals,” Phys. Rev. B **44,** 8496–8502 (1991).
20. Z. Lin, Z. Wang, C. Chen, and M.-H. Lee, “Mechanism for linear and nonlinear optical effects in monoclinic bismuth borate (BiB_3O_6) crystal,” J. Appl. Phys. **90,** 5585–5590 (2001).
21. D. N. Nikogosyan, *Nonlinear Optical Crystals: A Complete Survey* (Springer Media, 2005).
22. V. Wesemann, J. A. L‘Huillier, L. K. Friess, P. A. V. Loewis of Menar, G. Bitz, A. Borsutzky, R. Wallenstein, T. Salva, S. Vernay, and D. Rytz, “Optical properties of BiB_3O_6 with different phase matching orientations,” Appl. Phys. B **84,** 453–458 (2006).
23. J. Bromage, J. Rothhardt, S. Hädrich, C. Dorrer, C. Jocher, S. Demmler, J. Limpert, A. Tünnermann, and J. D. Zuegel, “Analysis and suppression of parasitic processes in noncollinear optical parametric amplifiers,” Opt. Express **19,** 16797–16808 (2011).
24. T. Lang, A. Harth, J. Matyschok, T. Binhammer, M. Schultze, and U. Morgner, “Impact of temporal, spatial and cascaded effects on the pulse formation in ultra-broadband parametric amplifiers,” Opt. Express **21,** 949–959 (2013).
25. F. Tavella, K. Schmid, N. Ishii, A. Marcinkevičius, L. Veisz, and F. Krausz, “High-dynamic range pulse-contrast measurements of a broadband optical parametric chirped-pulse amplifier,” Appl. Phys. B **81,** 753–756 (2005).
26. C. Manzoni, J. Moses, F. X. Kärtner, and G. Cerullo, “Excess quantum noise in optical parametric chirped-pulse amplification,” Opt. Express **19,** 8357–8366 (2011).
27. A. Alexandrovski, M. Fejer, A. Markosyan, and R. Route, “Photothermal common-path interferometry (PCI): new developments,” Proc. SPIE 7193, Solid State Lasers XVIII: Technology and Devices, 71930D (2009); doi:10.1117/12.814813.
28. B. Gronloh, P. Russbueldt, B. Jungbluth, and H.-D. Hoffmann, “Green sub-ps laser exceeding 400 W of average power,” Proc. SPIE 8959, Solid State Lasers XXIII: Technology and Devices, 89590T (2014); doi:10.1117/12.2041288.
29. J. Morikawa, C. Leong, T. Hashimoto, T. Ogawa, Y. Urata, S. Wada, M. Higuchi, and J.-i. Takahashi, “Thermal conductivity/diffusivity of Nd^{3+} doped $GdVO_4$, YVO_4, $LuVO_4$, and $Y_3Al_5O_{12}$ by temperature wave analysis,” J. Appl. Phys. **103,** 063522 (2008).
30. J. D. Beasley, “Thermal conductivities of some novel nonlinear optical materials,” Appl. Opt. **33,** 1000–1003

(1994).
31. D. Eimerl, L. Davis, S. Velsko, E. K. Graham, and A. Zalkin, “Optical, mechanical, and thermal properties of barium borate,” J. Appl. Phys. **62,** 1968–1983 (1987).
32. A. Klenke, S. Breitkopf, M. Kienel, T. Gottschall, T. Eidam, S. Hädrich, J. Rothhardt, J. Limpert, and A. Tünnermann, “530 W, 1.3 mJ, four-channel coherently combined femtosecond fiber chirped-pulse amplification system,” Opt. Lett. **38**, 2283–2285 (2013).
33. F. Zhuang, B. Jungbluth, B. Gronloh, H.-D. Hoffmann, and G. Zhang, “Dual-wavelength, continuous-wave Yb:YAG laser for high-resolution photothermal common-path interferometry,” Appl. Opt. **52,** 5171–5177 (2013).
34. J. H. Jang, I. H. Yoon, and C. S. Yoon, “Cause and repair of optical damage in nonlinear optical crystals of BiB_3O_6,” Optical Materials **31,** 781–783 (2009).
35. C. Rothhardt, J. Rothhardt, A. Klenke, T. Peschel, R. Eberhardt, J. Limpert, and A. Tünnermann, “BBO-sapphire sandwich structure for frequency conversion of high power lasers,” Opt. Mater. Express **4,** 1092–1103 (2014).
36. J. Matyschok, T. Lang, T. Binhammer, O. Prochnow, S. Rausch, M. Schultze, A. Harth, P. Rudawski, C. L. Arnold, A. L’Huillier, and U. Morgner, “Temporal and spatial effects inside a compact and CEP stabilized, few-cycle OPCPA system at high repetition rates,” Opt. Express **21,** 29656–29665 (2013).
37. K. Kato, “Temperature-Tuned 90° Phase-Matching Properties of LiB_3O_5,” IEEE J. Quant. Elec. **30**, 2950–2952 (1994).
38. H. Lingxiong, L. Xiang, Z. Ge, H. Chenghui, and W Yong, “The accurate refractive indices of BIBO crystal at different temperatures,” J. Phys. D: Appl. Phys. **42,** 225109 (2009).

---

1. Introduction

Optical parametric chirped-pulse amplification (OPCPA, [1–3]) has great potential for high average power amplification of ultrashort laser pulses, because the optical parametric amplification process does not rely on energy storage (population inversion) within the nonlinear crystals, and therefore has a reduced heat load. At an OPCPA-pump wavelength of 515 nm, OPCPAs are capable of delivering few-cycle pulses around a central wavelength of 800 nm at high average powers. So far, the highest demonstrated OPCPA average powers were 11.6 W [4] and 22 W [5], and in a pulsed operation 38.5 W during a burst [6]. These OPCPAs are made possible by the recent development of Yb-doped solid-state laser amplifier technologies (LMA/PCF-fiber [7], Innoslab [8], thin-disk [9, 10]) with sub-ps pulse durations demonstrating the potential to reach kilowatts of average power for OPCPA pumping at 515 nm. Such OPCPAs can be used as driving amplifiers for secondary sources in the field of attosecond technology and science [11]. For example, the Extreme Light Infrastructure – Attosecond Light Pulse Source (ELI-ALPS) in Hungary is planning a high power OPCPA operating at a repetition rate of 100 kHz with a pulse energy of up to 5 mJ and a pulse duration of sub-5 fs (1 mJ and sub-7 fs is planned in a first phase) [12, 13]. At such high average powers, however, the absorption of optical power within the crystals cannot be neglected. This leads to inhomogeneous heating of the nonlinear optical crystal and results in spatial temperature changes. Spatially inhomogeneous refractive index changes can occur, which lead to spatially varying phase-matching conditions, limiting the attainable average power, the spectral bandwidth [14], and the beam quality [13].

Borate crystals, such as beta-barium borate (β-BaB_2O_4, BBO) [4–6], lithium triborate (LiB_3O_5, LBO) [13] and bismuth triborate (BiB_3O_6, BiBO) [15], can be used for high average power OPCPAs. A comparison of the relevant optical properties for the crystals BBO, LBO and BiBO used in broadband parametric amplification is given in Table 1. All crystals have a comparably high effective nonlinear optical coefficient, d_{eff}. This allows for a high single-pass gain. All three crystals support a large spectral amplification bandwidth [16]. However, BiBO has a rather small energy band gap, E_g, which would make it susceptible to two-photon absorption at 515 nm. We would like to mention, that there are other nonlinear optical crystals with vast potential for high power applications, e.g. $YCa_4O(BO_3)_3$ (Yttrium Calcium Oxyborate - YCOB). This crystal can be grown to few-cm size, and its temperature tolerance and thermal conductivity are very high. However, its nonlinear coefficient is low [17], which requires the use of long crystals, limiting the attainable spectral bandwidth.

#206255 - $15.00 USD Received 18 Feb 2014; revised 8 May 2014; accepted 8 May 2014; published 14 Jul 2014

Table 1. Selected properties of nonlinear optical crystals [18]: d_{eff} nonlinear optical coefficient; ρ_{P} walk-off angle; $TT = \Delta T/\Delta k$ temperature tolerance, where ΔT is the change in temperature, and $\Delta k = k_{\mathrm{pump}} - k_{\mathrm{signal}} - k_{\mathrm{idler}}$ is the wave vector mismatch between pump, signal and idler waves; $AT = \Delta\theta/\Delta k$ angular tolerance, where $\Delta\theta$ is the variation of the phase-matching angle ($\lambda_{\mathrm{pump}} = 515$ nm, $\lambda_{\mathrm{signal}} = 800$ nm). The values for the bandgap E_{g} are experimental. The calculated values are in brackets [19–21].

	phase matching	d_{eff} (pm V^{-1})	ρ_{P} (mrad)	TT (K cm)	AT (mrad cm)	E_{g} (eV)
BBO	uniaxial	2.0	55.8	39.7	0.56	6.42(6.2)
LBO	biaxial	1.0	7.06	6.8	4.54	7.78(7.57)
BiBO	biaxial	3.0	24.6/25.1	2.74	1.15	4.32(3.45)

The OPCPA power scaling limits of borate crystals at a central wavelength of 800 nm will depend on their thermal properties. The current literature values of the linear absorption coefficients (α) at the OPCPA-pump wavelength at values near 515 nm are given as upper limit estimates: $\alpha < 10^4$ ppm cm^{-1} at 532 nm for BBO, and $\alpha < 10^3$ ppm cm^{-1} at 532 nm for LBO [21]. For BiBO, a value of $\alpha < 10^3$ ppm cm^{-1} was measured at 1064 nm [22], but so far no absorption coefficients have been reported in the green spectral region. Literature values for the thermal conductivity (κ) are available for BBO and LBO (see Table 2), but the thermal conductivities of BiBO along the main crystallographic axes x, y and z, and along the phase-matching direction have not been determined. For the numerical modeling and optimization of spatial temperature changes in the investigated borate crystals, the thermal conductivity (κ) and the wavelength-dependent linear absorption coefficients (α) at 515 nm are the most important parameters.

In general, signal, idler and pump waves are all subject to absorption. The signal wave around 800 nm is typically located in the center of the transparency window and exhibits very low absorption, which is typically negligible. The highest absorbed power is expected from the high power pump beam at 515 nm. Therefore, accurate knowledge of the absorption coefficients at this wavelength is highly desirable. Idler absorption can also considerably contribute to crystal heating; this heating can cause a longitudinal temperature change $\Delta T(r,z)$ along the beam propagation (z axis) [13]. Further contributions with lower impact to heating are expected from parasitic waves [23,24]. The highest contribution among parasitic effects is expected for amplified optical parametric fluorescence (AOPF). Its spectral bandwidth covers far into the infrared region where strong absorption (similar to the idler wave) takes place. AOPF generation and amplification can be avoided using a high seed (signal) energy in combination with moderate pump intensities [25,26].

In this paper, the three borate crystals, BBO, LBO, and BiBO, are investigated systematically for high power OPCPA applications and the scalability towards kW-level average power. In Section 2, up-to-date measurements of the thermal conductivities and the crystal absorption at the pump wavelength of 515 nm are presented. Two different methods were used: the photothermal common-path interferometry technique [27,28], and another method using thermal imaging measurements and finite element analysis to estimate the bulk absorption coefficient at high intensities. Next, numerical simulations were carried out to determine the influence of signal, idler and pump absorption on crystal heating under high power conditions (Section 3.1), and a finite-element analysis study was performed to clarify which crystal arrangement is more favorable for high power applications (Section 3.2). Finally, a discussion on possible limits to high average OPCPA power scaling is presented in Section 4.

2. Measurement of critical thermal properties of borate crystals

Thermal conductivity measurements were carried out on crystals purchased from Castech Inc. (China) and the crystals were 1×1×0.4 mm for LBO and BiBO, and 1×1×1 mm for BBO in size (Section 2.1). For the crystal absorption measurements at 515 nm (Section 2.2 and Section 2.3), three uncoated BBO crystals from different companies were purchased: (A) Castech Inc. (China), (B) Raicol Crystals Ltd. (Israel), and (C) A-Star Photonics Inc. (China). An additional, BBO crystal was purchased with protection-coating from company A, designated as (A-p), to assess the absorptive effect of the protective coating. Further, one LBO and one BiBO crystal (both uncoated, from A) were purchased. These crystals were 6×6×6 mm in size. References are provided for the conventional measurement methods. For the absorption measurement method using thermal imaging (Section 2.3), a detailed description in the text is provided.

2.1. *Thermal conductivity* κ

The thermal conductivity was determined according to $\kappa = D\rho c_{\mathrm{cp}}$, where the specific heat capacity, c_{cp}, and the density, ρ, were taken from literature. The thermal diffusivity, D, was measured using the temperature-wave analysis method [29] at the Institut für Laserphysik, Universität Hamburg, Germany. For BiBO, this was measured for the first time; in addition, the thermal conductivities of BBO and LBO in the phase matching (PM) direction were also measured. Other LBO and BBO values were taken from literature [21,30,31]. All results are listed in Table 2. The temperature dependence of the thermal conductivity was not measured. However, with the changes of temperature considered within Sections 3 and 4, expected changes in thermal conductivity should not change the broad conclusions of these Sections.

Table 2. Thermal conductivities at room temperature, $\kappa_{293\mathrm{K}}$, for BBO, LBO and BiBO crystals. Thermal conductivity was determined via thermal diffusivity measurements. These measurements were performed in the phase matching (PM) direction on BBO, LBO and BiBO samples, and in the main crystallographic planes for BiBO. Other thermal conductivity values were taken from literature [21,30,31].

	BBO	LBO	BiBO
$\kappa_{293\mathrm{K}}$ ($\mathrm{W\,m^{-1}K^{-1}}$)	$0.08/1.2\perp c$ [31]/ [30]	$2.7\parallel x$ [21]	$7.81\pm0.3\parallel x$
	$0.8/1.6\parallel c$	$3.1\parallel y$	$6.95\pm0.46\parallel y$
		$4.5\parallel z$	$17.32\pm0.92\parallel z$
$\kappa_{293\mathrm{K}}\parallel$ to PM dir.	0.97 ± 0.07	3.08 ± 0.03	10.54 ± 0.42

2.2. *Linear absorption coefficients (α_{515}): the photothermal common-path interferometry (PCI) method*

The linear absorption of the crystals was first characterized using a well established technique: photothermal common-path interferometry [27,28], measured at the Fraunhofer Institute for Laser Technology, Aachen, Germany. The crystal volume was locally heated using a 515 nm continuous wave laser with a beam diameter of 70 µm at an average power of 2 W. Figure 1 shows a typical measurement of the 515 nm absorption in a plane within the volume of an LBO crystal. The results are listed in Table 3, giving the averaged absorption at the front and back side of the crystal (beam input and output facet), and the averaged absorption coefficient α_{515} within the volume. In many surface cases, the standard deviation was larger than the averaged value. This does not stem from a poor signal-to-noise ratio of the PCI method, but rather an unequal distribution of absorption centers at the surface. In the case of BBO (C) (volume), a large error contribution came from the errors of the theoretically calculated material specific

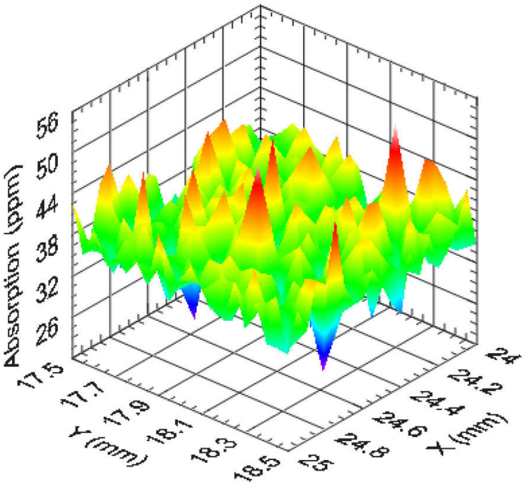

Fig. 1. An example measurement of a volume absorption of an LBO sample using the common-path interferometry method.

calibration factor, which relates the measured data to an absolute absorption for the bulk. In these cases, the error bars were adjusted so that no values were negative. Also stated are the ratios between absorption coefficients at 515 nm and 1030 nm. This information is important for high power second harmonic generation for OPCPA-pump pulse generation.

Table 3. Linear absorption coefficient, α_{515}, of BBO, LBO and BiBO measured with common path-interferometry at wavelength 515 nm. The values are averaged over the surface or volume. The superscripts are the standard deviations. A–C denote different companies (see text). BBO (A-p) is protection-coated; the remaining selected crystals were uncoated. $\alpha_{515}/\alpha_{1030}$: ratio between absorption coefficients at 515 nm and 1030 nm.

	front surface (ppm)	back surface (ppm)	volume (ppm cm^{-1})	$\alpha_{515}/\alpha_{1030}$
BBO (A-p)	$6.34^{(+8.70/-6.34)}$	$7.79^{(\pm 3.16)}$	$12.77^{(\pm 10.82)}$	0.61
BBO (B)	$4.78^{(+8.30/-4.78)}$	$4.90^{(+10.16/-4.9)}$	$42.78^{(\pm 28.65)}$	
BBO (C)	$37.57^{(\pm 26.43)}$	$9.57^{(+9.72/-9.57)}$	$226.5^{(+242.3/-226.5)}$	
LBO (A)	$0.32^{(+1.33/-0.32)}$	$0.25^{(+0.75/-0.25)}$	$37.33^{(\pm 3.91)}$	1.63
BiBO (A)	$37.97^{(\pm 30.24)}$	$20.74^{(+35.31/-20.74)}$	$312.1^{(\pm 149.7)}$	61.1

2.3. *Absorption coefficients (α_{515}) from thermal imaging measurements*

An alternative method for estimating the absorption coefficient (α_{515}) was developed using thermal imaging measurements. This measurement is not as precise as PCI. However, it is used to investigate the crystal absorption under high intensities, and therefore, would include other nonlinear and defect absorption effects. In summary, a thermally isolated crystal is irradiated by laser light under conditions similar to the real application, and in the steady state a thermal image is measured using an infrared camera. Thereafter, finite element analysis (FEA) of the crystal under stead-state irradiation was carried out with known laser and material parameters, and the averaged absorption as the free parameter. Figure 2(a) shows an example thermal image of a BBO(A) crystal irradiated at 515 nm, while Fig. 2(b) shows the corresponding FEA

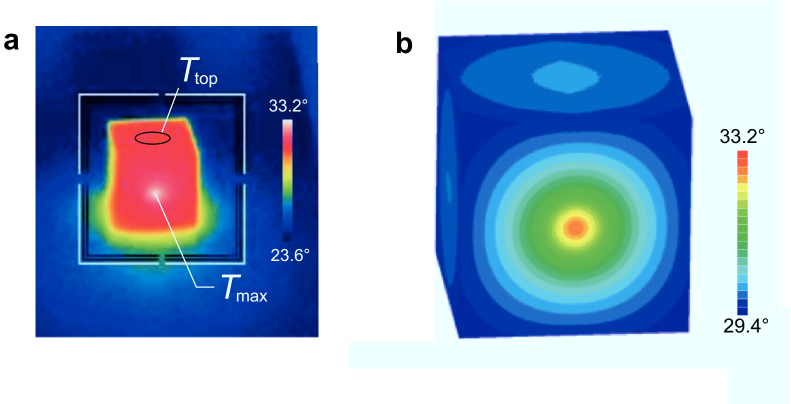

Fig. 2. An example absorption measurement using thermal imaging and corresponding simulation using FEA. (a) Thermal imaging of a nonlinear optical crystal upon irradiation with 120 W optical power at 515 nm (BBO (A), infrared camera FLIR-SC645) with peak temperature $T_{\max}$ and crystal boundary temperature T_{top}. (b) Finite element thermal steady-state analysis of the specific measurement in (a).

simulation. For this work, the measurements were carried out at the Helmholtz-Institut Jena, Germany.

The nonlinear optical crystals were irradiated using a high power frequency-doubled (515 nm) fiber laser system [32]. The parameters for irradiation were an optical power of $P = 120 \pm 4$ W, 1.5 ps pulse duration ($\sim$1 nm bandwidth), $M^2 < 1.5$ at a repetition rate of 1 MHz. The beam diameter was $d = 2.8 \pm 0.2$ mm at $1/e^2$. The crystals were placed on a 8 mm thick teflon sheet for thermal insulation. The temperature distribution on the crystal surface in thermal equilibrium was imaged using an infrared camera (FLIR-SC645).

A three-dimensional numerical FEA was performed in steady state using the package LISA (http://lisafea.com, Ver. 8.0.0). As the heat source within the crystals, a Gaussian beam was assumed and the simulation mesh grid included approximately 10^5 nodes. The main parameters used for the simulation were the thermal conductivity, κ, the emissivity, ε, the temperature at the crystal center, $T_{\max}$ (Fig. 2(a)), and the boundaries, T_{top} (Fig. 2(a)), and the heat transfer coefficient, h. A Neumann boundary condition was specified (same as the convective heat transfer) with a heat transfer coefficient h at the interface between the crystal and the boundary (air or heat sink). For an air boundary, free convection between the crystal surface and a static layer of air was assumed. The heat transfer coefficient was estimated using $h = Q/(A \cdot \delta T)$, where Q is the heat flow rate, A is the heat transfer surface, and δT is the difference between crystal surface and surrounding air temperature. The initial temperature for air or heat sinks was between 295–297 K. The initial crystal temperature was 295.9 K. The error for the measured peak temperature $\text{T}_{\max}$ in the crystal center was estimated over a 3×3 pixel area around the maximum. The measured temperature at the crystal boundary, T_{top}, was estimated at the crystal top (see thermal image in Fig. 2(a)) and has a large spread. This large spread results in a large error of the temperature change, ΔT, between the crystal center and the boundary. The remaining free parameter in the simulation, the heat flow rate Q, was optimized to fit the simulated temperature distribution to the experimentally measured distribution. From the optimum heat flow rate, the absorption coefficient could be estimated according to $\alpha_{515} = Q/(Pl_c)$. The results of this analysis for all crystals are given in Table 4.

#206255 - $15.00 USD Received 18 Feb 2014; revised 8 May 2014; accepted 8 May 2014; published 14 Jul 2014

Table 4. Absorption coefficients at 515 nm for BBO, LBO and BiBO, estimated via finite element analysis of the heat dissipation using photo-thermal imaging measurements. $T_{\max}$ is the temperature at the crystal (beam) center; ΔT is the temperature change from the center to the crystal surface; the incident pump power was 120±4 W. Surface reflections were taken into account for the simulations, and P_{tc} is the average transmitted pump power through the crystal. The error bars arise largely from the spread of ΔT. (a) The effect of the protective coating was studied comparing crystals BBO(A-p) and BBO(A). (b) Measurements of uncoated crystals.

		$T_{\max}$ (K)	ΔT (K)	P_{tc} (W)	α_{515} (ppm cm^{-1})
(a)	BBO(A-p)	304.8 ± 0.19	2.13 ± 0.45	116.0 ± 3.87	569 ± 146
	BBO (A)	303.2 ± 0.04	1.01 ± 0.25	112.0 ± 3.73	279 ± 80
(b)	BBO(B)	299.7 ± 0.02	0.46 ± 0.08	112.5 ± 3.75	127 ± 27
	LBO(A)	298.2 ± 0.02	0.10 ± 0.08	115.5 ± 3.85	86 ± 69
	BiBO(A)	421.0 ± 0.10	15.6 ± 2.50	109.0 ± 3.63	46100 ± 9300

2.4. Discussion of the absorption coefficients at 515 nm

The absorption coefficients of BBO vary substantially between manufacturers (Table 3 and Table 4). This depends to a large extent on the crystal growth process, the crystal purity and on the specific position of the crystal bulk in the boule, as for example reported for BiBO in [33]. In particular, for flux-grown crystals like most borates, the manufacturing process may strongly influence the quality and thus the thermal and parasitic absorption properties. Similar variations could be expected for BiBO; however, LBO can be mass produced relatively free of inclusions and might be produced more consistently.

Comparing the two absorption coefficient measurement methods, the absorption coefficients for BBO and LBO determined with the thermal imaging (Table 4) are higher compared to those from the PCI measurements (Table 3). The systematic differences can be explained by the different experimental conditions. The PCI measurements were performed punctually within the crystal volume, using a low power continuous wave laser. Here, large local variations of α_{515} were observed, and Table 3 lists only the mean values. In contrast, in the thermal imaging experiment, a high power, high intensity laser (2.25 GW cm^{-2}) was used and a large crystal volume was irradiated, which is more sensitive to local absorption maxima within the volume as well as on the surfaces. Furthermore, two-photon absorption (TPA) may occur at crystal defects due to bandgap lowering. Also at the crystal surfaces TPA might be possible. Most importantly, the absorption coefficients measured in our work were a factor of 10–100 lower than the upper limit values reported in the literature (BBO: $\alpha_{515} < 10^4$ ppm cm^{-1}, LBO: $\alpha_{515} < 10^3$ ppm cm^{-1}) [21].

In the case of BiBO, the absorption coefficient measured from thermal imaging differed substantially from the PCI results (cf. BiBO results in Table 3 and Table 4). This can be explained as follows: Two-photon absorption and photo-induced damages (color center formation) occur in BiBO upon pumping in the visible range at high peak intensities. The authors in [34] report on optical damage due to photorefraction, which can be repaired by annealing at higher temperatures. The two-photon absorption process energy for 515 nm photons is 4.8 eV, which is higher than the electronic bandgap of BiBO (Table 1). The effective absorption is given by $\alpha_{\mathrm{eff}} = \alpha + \beta I$, where β is the two-photon-absorption (TPA) coefficient. The pump intensity during the measurements was 2.25 GW cm^{-2}. With α_{515} from Table 3, and $\alpha_{\mathrm{eff}} = \alpha_{515}$ from Table 4, the TPA-coefficient for BiBO at 515 nm is estimated to be $\beta = 0.020 \pm 0.004$ cm GW^{-1}.

In Table 4(a), a direct comparison, between the coated BBO(A-p) and the uncoated BBO(A) from the same batch and manufacturer, determined a clear increase in absorption. This confirms the suggestion of using uncoated crystals for high power applications [14]. In Table 4(b), lowest absorption coefficient of BBO, $\alpha_{515} = 127\,\text{ppm}\,\text{cm}^{-1}$, is very close to the absorption coefficient of LBO, $\alpha_{515} = 86\,\text{ppm}\,\text{cm}^{-1}$.

3. Thermal simulations of high power OPCPAs and crystal heat-sink geometries

In this section, we first simulate a high power OPCPA stage, in order to determine the relative contributions of crystal heating from the signal, idler and pump waves (Section 3.1). In this case, a two-dimensional OPCPA model was applied. The parametric nonlinear coupled equations were solved within the slowly varying envelope approximation using a fourth-order Runge-Kutta split-step Fourier algorithm. Dispersion, self- and cross-phase modulation effects were taken into account as well as temperature dependent phase matching and inhomogeneous temperature distributions along the propagation axis and the radial axis; however, the temperature distribution is calculated analytically in this code assuming 1-dimensional radial symmetry. For the simulation an absorption coefficient of $100\,\text{ppm}\,\text{cm}^{-1}$ for LBO is assumed. In the case of LBO, this value is justified (see Table 3 and Table 4). The code is described in more detail in [13]. Second, based on the experience from the first simulation, we carry out a finite element analysis (FEA) and compare various heat-sink geometries using the FEA package LISA (http://lisafea.com/ Version 8.0.0) (Section 3.2).

3.1. Simulation of a high power OPCPA stage

The simulation parameters used were as follows. The pump wavelength was $\lambda_\text{P} = 515$ nm with a pump power $P_\text{P} = 1$ kW. The pump pulse duration was 0.6 ps. The LBO crystal (OPCPA stage) under consideration was pumped with an intensity of 85 GW/cm^2. Two signal (λ_S) bandwidths between 650–1000 nm and 700–1000 nm were compared, for cases (b.1) and (b.2), respectively (see Fig. 3). As a result, the corresponding idler bandwidth (λ_I with $1/\lambda_\text{I} = 1/\lambda_\text{P} - 1/\lambda_\text{S}$) was between 1062–2480 nm or 1062–1949 nm. The seed (starting signal) power was 1 W and the OPCPA gain was approximately a factor of 100, corresponding to 10% pump-to-signal conversion efficiency in a single pass. The crystal length was 2.3 mm. The radial crystal dimensions, r_c, were chosen to best fit the pump beam with low diffraction at the end facets and to reduce the radial temperature change to $d/r_\text{c} = 0.62$, where d is the beam diameter at $1/e^2$ intensity.

The idler absorption rate can exceed that of the pump wave, as it grows stronger along the beam propagation (z-axis), causing a longitudinal temperature change $\Delta T(z)$. In broadband OPCPA, the crystal thicknesses are on the order of $l_c = 1$ mm. Thus, the related longitudinal temperature changes are quite small, as shown in the cases (b.1) and (b.2) in Fig. 3(b), where $\Delta T_z = T_\text{max}(z = l_c) - T_\text{max}(z = 0) < 2$ K. This temperature change is not excessive but the maximum crystal temperature T_max is lower when the signal cutoff is at higher wavelengths ($T_\text{max} = 309$ K at $\lambda_\text{S,cut} = 700$ nm; $T_\text{max} = 336$ K at $\lambda_\text{S,cut} = 650$ nm). The idler wave generated from spectral signal components < 700 nm is strongly absorbed. Reducing the signal bandwidth in this wavelength range or shifting the signal bandwidth towards the infrared circumvents this problem [13, 14]. However, even if the signal seed is spectrally clipped, the amplified optical-parametric fluorescence (AOPF) may also contribute to strong absorption in the idler spectral region. Assuming a pump-to-signal conversion efficiency of 10%, an OPCPA signal-to-AOPF contrast of 10^{-3} as an upper limit [6] and an infrared absorption coefficient from Fig. 3(a), this provides $5 \times 10^{-5}\,\text{W}\,\text{cm}^{-1}$ of additional heat deposition from AOPF as an upper limit. This is about a factor of two lower than the pump wave absorption and can be considerably reduced by avoiding AOPF [25, 26].

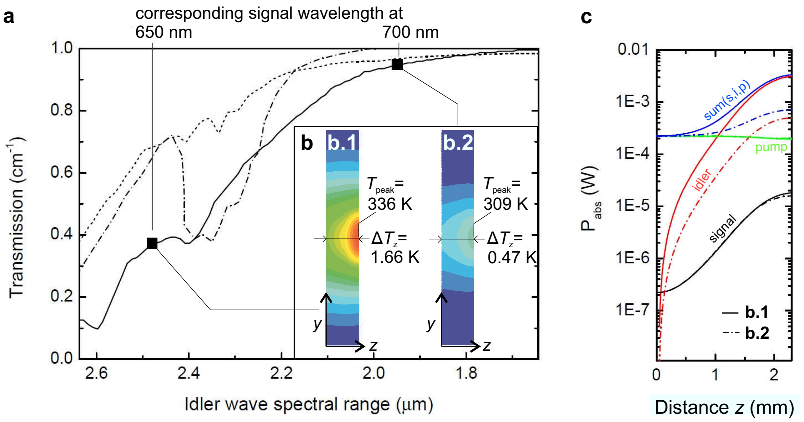

Fig. 3. Idler wave absorption in the optical parametric amplification. (a) Wavelength-dependent transmission in the infrared range of BBO (dash-dotted line), LBO (solid line) and BiBO (dotted line) [18]. (b) Temperature distribution of the combined pump, signal and idler wave absorption in LBO for two different spectral signal (and idler) cutoffs, as indicated in (a) as black rectangles, corresponding to 650 nm (b.1) and 700 nm (b.2). The absorbed power in both cases is shown in (c), leading to a maximum temperature $T_{\max}$ and a longitudinal temperature change ΔT_z, as denoted in the figure. (c) Absorbed optical power along the beam propagation (z-axis) of signal, idler and pump wave in LBO at signal cutoff wavelength of 650 nm (b.1, solid lines) and 700 nm (b.2, dash-dotted lines).

3.2. *Simulations of different heat-sink geometries*

The cooling of nonlinear optical crystals can be challenging because of their low heat transport coefficients. A finite element analysis (FEA) was performed for different cooling arrangements. In this case, no OPCPA simulation was carried out and we assumed a Gaussian beam heat source, with negligible idler absorption. A crystal size of 15×15×1 mm^3 was assumed. For this evaluation, BBO and LBO were considered owing to their superior thermal properties. For simplicity, the analysis was performed with a constant heat transfer coefficient for crystal-to-air, $h_{MA} = 10\ \mathrm{W\,m^{-2}\,K^{-1}}$. Further parameters were a thermal conductivity $\kappa = 401\ \mathrm{W\,m^{-1}\,K^{-1}}$ and $\kappa = 35\ \mathrm{W\,m^{-1}\,K^{-1}}$ for copper and sapphire, respectively, and a heat transfer coefficient for crystal-to-copper of $h_{MC} \approx 400\ \mathrm{W\ m^{-2}\,K^{-1}}$. The radial temperature change, $\Delta T_r = T_{\max}(\text{center}) - T(\text{boundary})$, was simulated between crystal center (maximum temperature) and the crystal boundary. In Fig. 4, the calculated temperature distributions of three different cases are shown for an absorbed optical power of 0.1 W. The cases are free standing geometry (a.1), copper heat sinks at the side boundaries (a.2), and a sandwich structure with optically bonded sapphire plates at the front and back surface (a.3).

Case (a.1) represents the simplest option. However, cooling the crystal by air convection causes turbulent airflow leading to beam pointing variations. The crystal heats up to a peak temperature $T_{\max} = 332\,\mathrm{K}$ with a radial change of $\Delta T_r = 19\,\mathrm{K}$. In case (a.2), efficient heat removal off the crystal sides is achieved by mounting copper heat sinks at the sides of the crystal. Compared to case (a.1), this reduces the peak temperature to $T_{\max} = 319\,\mathrm{K}$, while the radial change is slightly increased, $\Delta T_r = 23\,\mathrm{K}$. The limitations were given by the large crystal aperture (front and back surfaces), which in the case discussed here led to a large uncooled surface area. A significant improvement can be achieved by optical bonding thin sapphire plates at the front and rear surface of the BBO crystal, as recently suggested in [14]. Since sapphire provides a 40 times larger thermal conductivity, compared to BBO, the generated heat is dissipated more

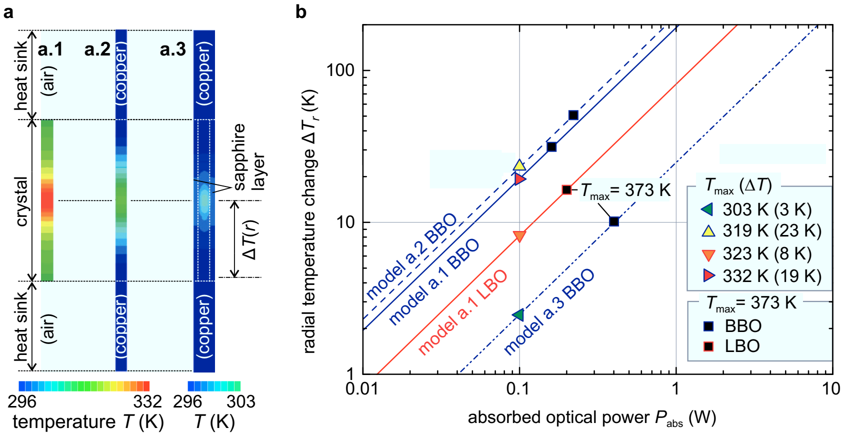

Fig. 4. Radial temperature change ΔT_r in nonlinear optical crystals. (a) Temperature distribution in radial (vertical) and beam propagation direction (horizontal) in a BBO crystal for different cooling arrangements, calculated for 0.1 W of absorbed optical power using finite element analysis. Case a.1: free standing crystal ($\Delta T_r = 19$ K); case a.2: crystal with thermally contacted copper heat sink ($\Delta T_r = 23$ K); case a.3: same as in a.2 with additional optically contacted 500 µm sapphire layers on the front and rear crystal facets ($\Delta T_r = 3$ K). (b) Radial temperature change ΔT_r with varying absorbed optical power P_{abs} for different cooling arrangements a.1 (solid lines), a.2 (dashed lines) and a.3 (dotted-dashed lines) and for different crystals (BBO blue lines, LBO red lines). In the case of $P_{abs} = 0.1$ W, the peak temperatures T_{max} and the maximum radial temperature changes ΔT_r are calculated (triangles, see legend). The selected cases with a peak temperature of $T_{max} = 373$ K are shown (black squares).

efficiently. Such a BBO-sapphire sandwich structure has already been manufactured successfully and tested in high power SHG experiments [35]. Note that a similar solution is currently not available for LBO. In this work, such a sandwich structure was simulated with FEA (case (a.3)). The radial temperature change and the peak temperature could be efficiently reduced, yielding $T_{max} = 303$ K, and $\Delta T_r = 3$ K (Fig. 4(a)).

The performance of the three heat-sink geometries for BBO is compared in Fig. 4(b), where the radial temperature changes ΔT_r are simulated for different absorbed optical power P_{abs} (blue lines). The total absorbed power depends linearly on the crystal length, if only pump wave absorption is considered. The cases discussed above are marked as triangles (see legend). In addition, the simulation for LBO in free standing geometry (case (a.1)) is also shown (red line). In free standing geometry, the heat removal in LBO is more efficient than in BBO. Because of the higher thermal conductivity of LBO, a lower peak temperature and a smaller radial temperature was attained. The best configuration is the sandwich structure (Fig. 4(a), case (a.3)).

4. Discussion on power scaling limits

The power limits on the output from a single OPCPA stage are given by thermal effects. At high powers, the signal spectrum, due to idler absorption in the infrared, will have to be restricted to values above 700 nm, as discussed in Section 3.1. In addition, other parasitic effects such as AOPF (Section 3.1) and weak parasitic frequency mixing [36], for example, in the ultraviolet spectral region can also be neglected. We therefore only need to consider the absorption of the OPCPA-pump at 515 nm. While this paper has improved knowledge of this parameter, knowledge of the temperature dependence of other parameters are not known: for example, the thermo-optic coefficient for refractive indices reported in scientific literature are valid for temperatures $T = 293$–353 K for BBO [31], $T = 293$–383 K for LBO [37] and for BiBO for temperatures $T = 303$–443 K [38]. Thus, we restrict our average power scaling estimates to temperatures below $T_{\mathrm{peak}} = 373\,\mathrm{K}$ (Fig. 4(b), black rectangles).

Crystal fracture can be a difficult effect to model. For example, for BBO Eimerl *et al.* [31] calculated a longitudinal fracture temperature of 170°C for a thin plate with a surface orientation normal to $\theta = 22^\circ$ and $\phi = 90^\circ$, which is used for phase matching of the OPAs. However, in our case, the temperature changes are mainly in radial direction. Further, the fracture toughness depends strongly on surface defects. For example, BBO crystal damage was observed in [14], at a radial temperature change of $\Delta T_r = 50$ K over a crystal aperture of 5 mm.

More critical is the phase-matching change driven by thermal effects. Thermal dephasing is expressed as

$$\delta(\lambda_{\mathrm{signal}}, T) = \frac{1}{2}|\Delta k(\lambda_{\mathrm{signal}}, T)| l_{\mathrm{c}}, \tag{1}$$

where $|\Delta k(\lambda_{\mathrm{signal}}, T)|$ is the absolute phase mismatch at the signal wavelength, $\lambda_{\mathrm{signal}}$, T is the crystal temperature and l_{c} is the nonlinear crystal length. Using broadband phase-matching, a large signal bandwidth is amplified if $\delta(\lambda_{\mathrm{signal}}, T) < \pi/2$. A thermally induced change of the phase-matching will result in a decrease of the gain for certain wavelengths with $\delta(\lambda_{\mathrm{signal}}, T + \Delta T(r)) > \pi/2$, where $\Delta T(r) = T_{\mathrm{max}} - T(r)$ is the radial temperature change. This causes a radially dependent thermal dephasing, $\delta(\lambda_{\mathrm{signal}}, r)$, and thus a radially varying bandwidth $\Delta\lambda_{\mathrm{signal}}(r)$, pump-to-signal conversion efficiency $\eta(r)$, and radially dependent group velocity $v_{\mathrm{g}}(r)$. For a signal bandwidth of $\Delta\lambda = 300\,\mathrm{nm}$, around 820 nm center wavelength, thermal dephasing limits were calculated for 1.2 mm BBO, 2.3 mm LBO and 0.82 mm BiBO (typical values for single-stage high power OPCPAs). These limits, $\langle\Delta(T)\rangle = \pi/2$, were estimated to be about $\Delta T = 125$ K for BBO, 36 K for LBO, and 17 K for BiBO. These values provide rough estimates of allowed maximum changes in crystal temperature.

Now, if we assume a OPCPA-pump power of 10 kW, free standing BBO (case (a.1), see Section 3.2) with $\alpha_{515} = 127\,\mathrm{ppm\,cm^{-1}}$ and $l_{\mathrm{c}} = 1.2$ mm would lead to an absorbed heat of $P_{\mathrm{abs}} = 0.15$ W, resulting in a radial change of $\Delta T_r = 30$ K. In the case of a $l_{\mathrm{c}} = 2.3$ mm long, free standing LBO (case (a.1)) with $\alpha_{515} = 86\,\mathrm{ppm\,cm^{-1}}$ pumped at 10 kW average power, about $P_{\mathrm{abs}} = 0.2$ W are absorbed, leading to an uncritical radial change of $\Delta T_r = 16$ K. This result for LBO is supported by detailed numerical simulations, which demonstrate a negligible change to critical laser parameters, such as, signal energy, bandwidth and beam profile for a similar radial change in temperature [13]. In the case of a BBO sandwich structure with sapphire layers (case (a.3)), an average power of 116 kW would lead to an absorbed heat of $P_{\mathrm{abs}} = 1.2$ W, resulting in an uncritical radial change of $\Delta T_r = 30$ K. At these OPCPA-pump powers, the radial changes in temperature are well below the thermal dephasing limits calculated above. Finally, if we assume a pump-to-signal conversion efficiency of 10%, a few-cycle laser pulse could be generated with kW-level of average power for free standing BBO and LBO (case (a.1)), and above 10 kW for a BBO sandwich structure (case (a.3)).

For ranking of the nonlinear crystals for high power applications, we define a figure of merit, $G_T = \alpha_{515}/(TT_{300} \cdot \kappa)$ in units $\mathrm{kW^{-1}cm^{-1}}$: a lower value is better. The corresponding values are $0.33\,\mathrm{kW^{-1}cm^{-1}}$ for BBO(B), $0.41\,\mathrm{kW^{-1}cm^{-1}}$ for LBO(A) and $160\,\mathrm{kW^{-1}cm^{-1}}$ for BiBO(A) using the thermal conductivities in the phase-matching direction (Table 2.1) and the absorption coefficients from Table 4.

5. Conclusion

This work delivers up-to-date values for the absorption coefficients at 515 nm for the borate crystals: BBO, LBO and BiBO. They were measured with the well established, photothermal

Received 18 Feb 2014; revised 8 May 2014; accepted 8 May 2014; published 14 Jul 2014

common-path interferometry method (Section 2.2). The results demonstrate a large variation of absorption values within and on the surface of the crystal (Fig. 1). Additionally, in the case of BBO there would appear to be a large variation between manufacturers. Compared to literature values, which were only given as upper limits, these values are about 1–2 orders of magnitude lower. There are two possible explanations for this discrepancy: (i) improved crystal growing and handling methods, and (ii) the accuracy of the PCI method. Other methods only give an upper limit. For example, BiBO was measured at 1064 nm using a resonator-based method [22], which suffers from misinterpreting scatter or reflection loss for absorption. In order to confirm these results, another method was developed using thermal imagining at high intensities (Section 2.3). This method provides an absorption value averaged over the crystal and is susceptible to various nonlinear absorption processes at the surfaces and in the bulk. The values were found to be greater than the values measured by PCI but still much lower than the literature upper limits. In addition, from the measurement it was possible to estimate the two-photo absorption of BiBO at 515 nm. This work also delivered values for the thermal conductivities of BBO, LBO and BiBO nonlinear crystals in phase-matching directions, as well as, for the first time, for BiBO crystals along the main crystallographic axes. For the application of these crystals to high power OPCPAs, crystals have to be individually selected for minimum pump wave absorption. We suggest, that the crystal characterization be performed under experimental conditions, i.e. at high intensity and high average power, where the absorption is more sensitive to nonlinear effects. The application of BiBO is limited by two-photon absorption at 515 nm.

Numerical simulations were carried out in order to demonstrate the relative contributions of the signal, idler and pump pulses. It was shown that the major contribution to heat deposition within the crystals originates from the pump beam absorption at 515 nm wavelength, provided that the signal spectrum is cut off below 700 nm, thus preventing a strong idler infrared absorption. Assuming crystal heating through absorption of a Gaussian pump beam, the OPCPA-pump average power is mainly limited by radial temperature changes. Concerning the radial phase-matching changes, BBO and LBO are best suited for broad bandwidth, high power OPCPA, representing the best compromise between temperature tolerance and heat dissipation. The choice for one of these crystals depends on the specific application. Finite element analysis was performed on different heat-sink geometries. Free standing crystals were found to have slightly smaller temperature changes compared to crystals with a thermally contacted copper heat sink, but had a higher maximum temperature at the center. The best geometry was found to be a BBO-sandwich structure, which has recently been fabricated successfully [35]. Finally, assuming a pump-to-signal conversion efficiency of 10%, a few-cycle laser pulse could be generated with above kW-level of average power.

Received 18 Feb 2014; revised 8 May 2014; accepted 8 May 2014; published 14 Jul 2014